Tellus (1991), *43A*, 128–144

An observational study of the energy transfer between the seasonal mean flow and transient eddies

By JIAN SHENG and JACQUES DEROME, *Department of Meteorology, McGill University, 805 Sherbrooke Street West, Montréal, Québec, Canada, H3A 2K6*

(Manuscript received 29 November 1989; in final form 24 September 1990)

ABSTRACT

The large-scale energetics of the Northern Hemisphere atmospheric motions are computed in the frequency domain using a 5-year data set from the ECMWF operational analyses. The geographical distributions of kinetic energy (*KE*) for the fast transient (periods shorter than 10 days) assume the shape of elongated bands indicating the structure of the storm tracks. The slow transients (periods longer than 10 days) exhibit local maxima of *KE* over the eastern regions of the major oceans. The slow transient available potential energy (*APE*), on the other hand, displays maxima over the American and Asian continents. Both baroclinic and nonlinear conversions are responsible for the maintenance of low-frequency disturbances when hemispherically-integrated quantities are considered. Low-frequency disturbances over the land are maintained primarily through baroclinic energy conversions, while those over the oceans are maintained primarily through a barotropic energy transfer from the seasonal mean flow and through a nonlinear energy transfer from high frequency eddies. With the flow separated in terms of three frequency "bands", namely, the seasonal mean, the low- and the high-frequency eddies, the energy cycle is a rather simple one. During summer, (i) the *APE* flows from lower to higher frequency bands, (ii) the baroclinic conversion transforms *APE* to *KE* for all frequency bands, and finally, (iii) *KE* flows from higher to lower frequencies (including the time-mean flow). For the winter season, the energy flows in the same direction, except for one transfer, the exchange of *KE* between the time-mean flow and the slow transients. The direction is from the time-mean flow to the slow transients, which is presumably due to the time-mean motions being barotropically unstable during the winter.

1. Introduction

In recent papers by Sheng and Hayashi (1990a, b), the atmospheric energetics were studied spectrally in the frequency domain with a focus on the energy balance of low frequency disturbances. To study the energy cycle in terms of kinetic energy (*KE*) and available potential energy (*APE*), the transient fluctuations were divided at a period of 10 days into low- and high-frequency (synoptic time scale) groups. The choice of the 10-day period is related to the fact that eddies with periods longer than 10 days gain *KE* and lose *APE* while those with periods shorter than 10 days lose *KE* and gain *APE* from exchanges among frequencies. It was shown that the energy balance for low frequency transients is quite different from that of the higher frequency ones. Transients with a synoptic time scale are energetically typical of those predicted by the baroclinic instability theory (Charney, 1947; Eady, 1949), i.e., the time-mean *APE* is converted to synoptic scale *APE*, which is in turn converted to transient *KE*. The maintenance of low frequency transients, however, is complicated by the fact that, although the baroclinic energy conversion is an important *KE* source, nonlinear exchanges of *KE* between the slow and fast transients also play a significant role. Data analyses, both from atmospheric observations and general circulation models (GCMs), indicate a systematic flow of *KE* from high frequency bands to low frequency bands. This type of energy decascade is reminiscent of the non-linear energy exchange in the wavenumber domain (Saltzman, 1970; Chen and Wiin-Nielsen, 1978).

Simmons et al. (1983) proposed a theory for the

existence of low frequency transient variability. In a linear stability analysis of a barotropic model having a realistic zonally and meridionally varying winter-time basic state, the most rapidly growing modes were found to be those related to the observed "Pacific/North American" and "East Atlantic" teleconnection patterns. The mechanism by which the slow transients extract kinetic energy from the time-mean flow is through the down-gradient flow of zonal momentum in the jet-exit regions. It is, therefore, a two-dimensional barotropic instability which differs fundamentally from the classical theory of a zonally symmetric barotropic jet (Kuo, 1949). Wallace and Lau (1985) tested this concept with several observational data sets consisting of Northern Hemisphere winters. In a systematic analysis of the structure and horizontal distributions of eddy transients for the high- and low-frequency bands, they positively identified the importance of barotropic instability in the generation of slow transients. It was shown that the winter time-mean flow at the 300 mb level barotropically supplies *KE* to low frequency transients, but extracts *KE* from high frequency disturbances.

In the energy calculations of Sheng and Hayashi (1990a, b), however, the barotropic exchange of kinetic energy between the time-mean flow and the transient eddies is of less importance. The transient eddies lose a small amount of *KE* (small in comparison with the baroclinic conversion) to the time-mean flow in both the high- and low-frequency ranges. The analyses of Sheng and Hayashi used multi-level data sets and a more complete set of equations than those of Wallace and Lau. On the other hand, the fundamental difference between the two studies is perhaps due to the use of an annual mean flow in Sheng and Hayashi rather than the winter mean as used in Wallace and Lau. The first purpose of this study is therefore to recalculate the energetics in the frequency domain separately for the winter and summer seasons and contrast the results, in the hope of obtaining a more comprehensive view of the energetics of slow transients.

In most earlier work (e.g., Lorenz, 1967), general circulation statistics were presented in a zonally averaged format, which precluded any study of longitudinal differences. Recently (e.g., Blackmon et al., 1977), analyses were extended with some emphasis being placed on examining the longitudinal distributions of the contributions to the energy integrals. The results clearly illustrated that general circulation statistics exhibit strong longitudinal variations and geographical patterns. The latitude-pressure cross-sections of energy parameters were discussed in Sheng and Hayashi (1990b). It is of great interest that the direction of nonlinear *KE* exchange reverses its sign from the mid-latitudes to the tropics. Instead of being enhanced, the slow transients are actually damped by the fast transients in low latitudes. To further explore the processes responsible for the existence of slow transients, the geographical distributions of energetics in the frequency domain are examined in this paper.

In Section 2 the scheme and data set used in this study are briefly reviewed. The contrast of hemispherically integrated energetics between the winter and summer seasons is discussed in Section 3. The geographical distributions of energy and energy conversion terms are presented in Sections 4 and 5, for the winter and summer seasons, respectively. The results are summarized in Section 6.

2. Energy equations in the frequency domain and data analysis procedure

The form of the spectral energy equations in the frequency domain used in the present study is a variation of those discussed in Hayashi (1980) and Sheng and Hayashi (1990a). The formulation invokes the use of the cross-spectral technique to compute the nonlinear advection and curvature terms in the governing equations. In comparison with the conventional method of convolution in the frequency domain, the scheme effectively reduces the amount of calculations involved. The *KE* and *APE* equations in the frequency domain can be written as,

$$LK^{\ell} + NK^{\ell} + AK^{\ell} + FK^{\ell} + FP^{\ell} - D^{\ell} = 0, \quad (1)$$

$$LK^{\mathrm{h}} + NK^{\mathrm{h}} + AK^{\mathrm{h}} + FK^{\mathrm{h}} + FP^{\mathrm{h}} - D^{\mathrm{h}} = 0, \quad (2)$$

$$LA^{\ell} + NA^{\ell} - AK^{\ell} + FA^{\ell} + G^{\ell} = 0 \quad (3)$$

$$LA^{\mathrm{h}} + NA^{\mathrm{h}} - AK^{\mathrm{h}} + FA^{\mathrm{h}} + G^{\mathrm{h}} = 0. \quad (4)$$

Here the superscripts ℓ and h denote the energy transfer terms for the low- and high-frequency

Tellus A 43/2-4

bands, respectively. The various terms in eqs. (1) through (4) are interpreted as follows:

AK baroclinic conversion from *APE* to *KE*
D dissipation of transient *KE*
FA convergence of the transient *APE* flux
FK convergence of the transient *KE* flux
FP convergence of the transient flux of potential energy
G generation of transient *APE*
LA transfer of *APE* from the time-mean flow to the transient eddies
LK transfer of *KE* from the time-mean flow to the transient eddies
NA transfer of *APE* due to nonlinear interactions of transient eddies
NK transfer of *KE* due to nonlinear interactions of transient eddies.

The mathematical expression for each term is given in Appendix A and a list of the symbols used in the above equations can be found in Appendix B.

The data set used in this study is taken from the operational analyses of the European Centre for Medium Range Weather Forecasts (ECMWF). From the original data set, the geopotential heights and temperatures at the 100, 200, 300, 500, 700, 850, and 1000 mb pressure levels were extracted, on a 5° longitude-latitude mesh, at an interval of 24 h. The data set starts at 12 GMT 1 January 1980 and ends on 12 GMT 31 December 1984. The same data were used by Sheng and Hayashi (1990b). The vertical velocity component was calculated kinematically through the use of the continuity equation with values of the calculated horizontal divergence corrected by the method suggested by O'Brien (1970). The horizontal divergence of the ECMWF analyses was too weak during the period of 1980–1982, especially over the tropics (Trenberth and Olson, 1988). It was pointed out in Sheng (1986) and Sheng and Hayashi (1990b) that even with the kinematic vertical velocity the baroclinic conversion *AK* is still likely to be underestimated. On the other hand, Sheng and Hayashi (1990a) indicated that the significant disagreement of *AK* estimates between the ECMWF and GFDL (Geophysical Fluid Dynamics Laboratory) datasets is largely due to the discrepancies of the divergent components associated with the time mean and annual cycles.

In this study the time-mean flow is defined as the 120-day time average, starting from 16 November for the winter season, and from 16 May for the summer season. The seasonal variation has been excluded from the transient flow by removing the first four Fourier harmonics of the annual cycle from the entire time series, following Blackmon et al. (1977). Hence, the frequency range of the present analysis corresponds to periods between about 2 and 90 days. Due to the lack of direct measurements of atmospheric diabatic heating and dissipation, the *G* and *D* terms in eqs. (1) through (4) were computed as residuals required for an assumed balance.

3. Comparison of energetics between the summer and winter seasons

The winter and summer distributions of *KE*, *APE* and *AK* in the frequency domain are shown in Table 1. Each period range corresponds to constant intervals in log-frequency, and the values represent integrals over the intervals. The advantage of this presentation has been discussed in Sheng and Hayashi (1990a). All the values have been averaged over the entire mass of the Northern Hemisphere, the units being J/m^2 for *APE* and *KE*, and W/m^2 for the energy conversion terms.

The distribution of *KE* is characterized by a pronounced energy concentration in the mean flow. Approximately 61 percent during winter, and 44 percent during summer, of the total *KE* is due to

Table 1. *Hemispherically integrated energetics for the winter and summer (in parentheses) seasons*

Periods (days)	*KE* (10^4 J/m^2)	*APE* (10^4 J/m^2)	*AK* (W/m^2)
Time-mean	98 (29)	500 (179)	0.387 (0.841)
77–120	0.4 (0.4)	0.7 (0.5)	0.006 (0.002)
51–77	3.8 (2.8)	3.7 (2.1)	0.002 (0.011)
34–51	4.7 (2.6)	3.9 (1.9)	0.062 (0.013)
23–34	6.3 (3.8)	4.7 (2.7)	0.057 (0.031)
15–23	6.1 (4.7)	4.5 (2.2)	0.083 (0.047)
10–15	8.3 (5.2)	5.1 (3.1)	0.125 (0.060)
6.8–10	8.4 (5.3)	5.2 (2.5)	0.147 (0.086)
4.5–6.8	8.6 (4.4)	4.5 (2.4)	0.223 (0.091)
3.0–4.5	8.1 (4.2)	3.7 (1.9)	0.287 (0.096)
2.0–3.0	7.3 (3.4)	2.9 (1.6)	0.269 (0.084)

time independent flows. On the other hand, a broad maximum occurs in the high frequency region for both seasons. These features are consistent with the results of Sheng and Hayashi (1990a) from the FGGE year. In comparison with the annual mean value for the FGGE year, it is apparent that, by removing the seasonal cycle, as described in Section 2, the energy level of the transients with periods longer than 77 days is significantly reduced, but is virtually unchanged at the high-frequency end (Sheng and Hayashi, 1990a, Fig. 8).

A comparison of seasonal energetics indicates that the levels of *KE*, *APE* and *AK* in all frequency bands are higher during the winter than during the summer. However, the low frequency transients appear to experience a relatively moderate seasonal variation in comparison with the high frequency eddies. It is understood that the strong seasonal contrast in high frequency transient activity is closely related to the seasonal contrast in the baroclinicity of the atmosphere. Strong winter disturbances are a direct consequence of larger vertical wind shears and horizontal temperature gradients in the troposphere. On the other hand, the present result suggests a weaker dependence of slow transients upon baroclinicity. Another interesting observation is the shift in the frequency of the energy peaks between the two seasons. In the winter, both *KE* and *APE* peak at somewhat higher frequencies than in the summer. This can be explained by the stronger westerlies that occur during the cold season. Due to the effect of horizontal advection, the majority of eastward-moving disturbances tend to speed up during the winter, and therefore more energy is associated with the high frequency eddies.

Following Sheng and Hayashi (1990a, b) the energy cycles for the winter and summer seasons are summarized in Fig. 1 by regrouping the spectra into motions of the time-mean, the low frequencies, which represents approximately the periods between the synoptic time scales and about 90 days, and the high frequencies, which represent synoptic time scales shorter than 10 days. A similar analysis calculated from the yearly data, which include all 12 months in the time series, was given in Sheng and Hayashi (1990b). Each box in a given figure represents an energy resevoir of the labeled form and frequency range and contains the amount of energy shown in the bottom of the box

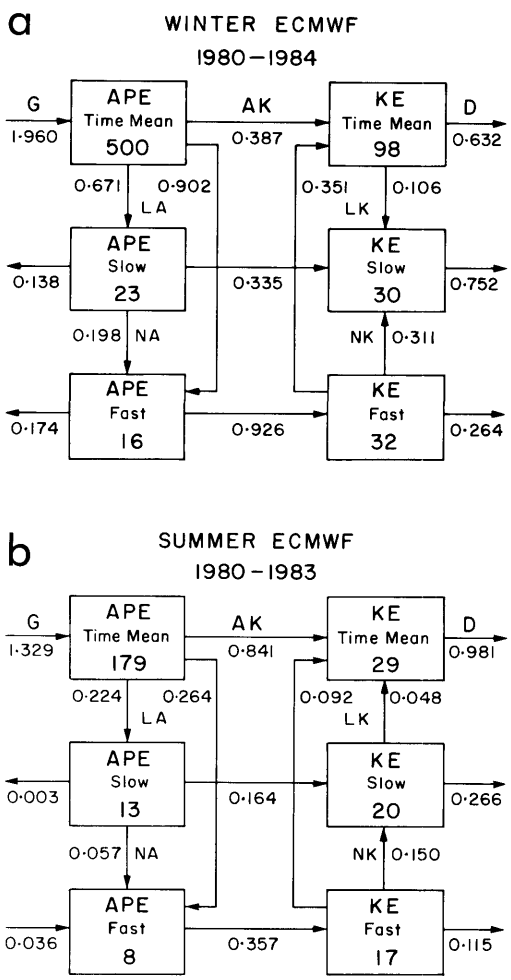

Fig. 1. Schematic depiction of the atmospheric energy cycle in the frequency domain. The numbers in boxes denote the energy storage in units of 10^4 J/m^2, and the arrows represent energy conversions or exchanges in W/m^2 for (a) winter and (b) summer. The annual-mean estimates are given in Fig. 8 of Sheng and Hayashi (1990b).

in units of 10^4 J/m^2. The arrows indicate the directions of the energy flow while the values next to the arrows give the magnitudes of the energy transfer in units of W/m^2. These three energy cycles (Fig. 1a, b, and Fig. 8 in Sheng and Hayashi, 1990b) depicted are very similar and are consistent with the analyses of the FGGE year data processed at the ECMWF and GFDL (Sheng and Hayashi, 1990a). The general picture revealed by

the calculation is one of available potential energy being generated by diabatic heating largely in the time-mean flow and flowing to transient disturbances of both high and low frequencies through the eddy heat transfer processes measured by *LA*. A smaller amount of *APE* is also transferred down to shorter time scales by the nonlinear exchanges, *NA*. The results also indicate that potential energy is converted to kinetic energy at all frequency groups. It should be noted that significantly more energy is converted in the fast transient group than the slow transient group. Through nonlinear exchanges measured by *NK*, kinetic energy is then transferred to longer time scales. A salient feature that distinguishes the energy balance of the slow transients from that of the fast transients is that the baroclinic conversion, although still important, is no longer the unique energy source for the slow transient *KE*. Important contributions also come from *NK*, and to some extent, from *LK*, as will be evident in the discussion of local energy contributions presented in Sections 4 and 5.

The seasonal contrast of energy cycles can be summarized simply by noting that higher energy levels and energy conversions are observed in the winter than in the summer while the general directions of the energy flow remain unchanged, with a few exceptions that are now discussed. First, the baroclinic conversion for the time-mean flow is weaker in the winter season. A closer inspection reveals that the hemispheric mean value of this term results from the close competition between the positive contribution from the lower latitudes where the Hadley cells prevail, and the negative contribution from the extratropics. In the summer, as the Southern Hemisphere Hadley cell extends slightly northward across the equator, the positive contribution from the tropics is significantly increased.

Another exception is the seasonal reversal of the barotropic conversion *LK* in the low-frequency range. Consistent with the results of Wallace and Lau (1985), the *LK* term during the cold season is positive, indicating an energy transfer to the slow transients (Fig. 1a). The magnitude of the conversion, however, is small so that it would take the mean flow about 33 days to replenish the *KE* reservoir. An estimate of 14 days was obtained by Wallace and Lau, based upon 300 mb data only. On the other hand, the calculations of *AK* and *NK* yield amplification times of 10 and 11 days, respectively. These terms, however, show significant geographic dependence, as will be discussed in the next two sections. It is of interest that during the summer the seasonal mean flow extracts *KE* from the slow transients and appears to be barotropically stable (Fig. 1b). According to the detailed analysis of Wallace and Lau, it is the zonal asymmetry of the winter stationary waves that overcomes the contribution from the convergence of meridional momentum flux into the jet stream and provides the net supply of *KE* to the slow transients. In view of the present results, the strengths of the summer stationary waves does not appear large enough for the convergence of zonal momentum flux to be dominant in *LK*, and the same can be stated for the annual mean case (Sheng and Hayashi, 1990b, Fig. 8).

4. Local contributions to the winter energetics

The main interest in this section is the local contributions of spectral energetics to the maintenance of transient eddies with either short or long periods. In the presentation that follows, a contrast is drawn between the fast and the slow transients. All quantities shown have been vertically integrated and have units of J/m^2 for the energy levels and W/m^2 for the conversion terms. Since the circulation statistics involve either high order moments or spatial derivatives, the results are rather noisy and have been spectrally filtered by retaining spherical harmonics triangularly truncated at zonal wavenumber 12. The weakly filtered data contain at least 85 percent of their original variance.

Fig. 2a shows the distribution of the kinetic energy during the Northern Hemisphere winter for transients with periods shorter than 10 days. It is characterized by elongated maxima over the western Atlantic around 40°N and the central Pacific at slightly lower latitude. The zone of maximum values in the Atlantic is oriented in a somewhat northeast-southwest direction. These two regions were previously shown by Blackmon et al. (1977) to be areas of local maxima in the high frequency transient variance of the geopotential height and identified as storm tracks. The latter are found downstream and slightly poleward of the 200 mb jet stream, where the baroclinicity is most intense. A third region of high variance, though

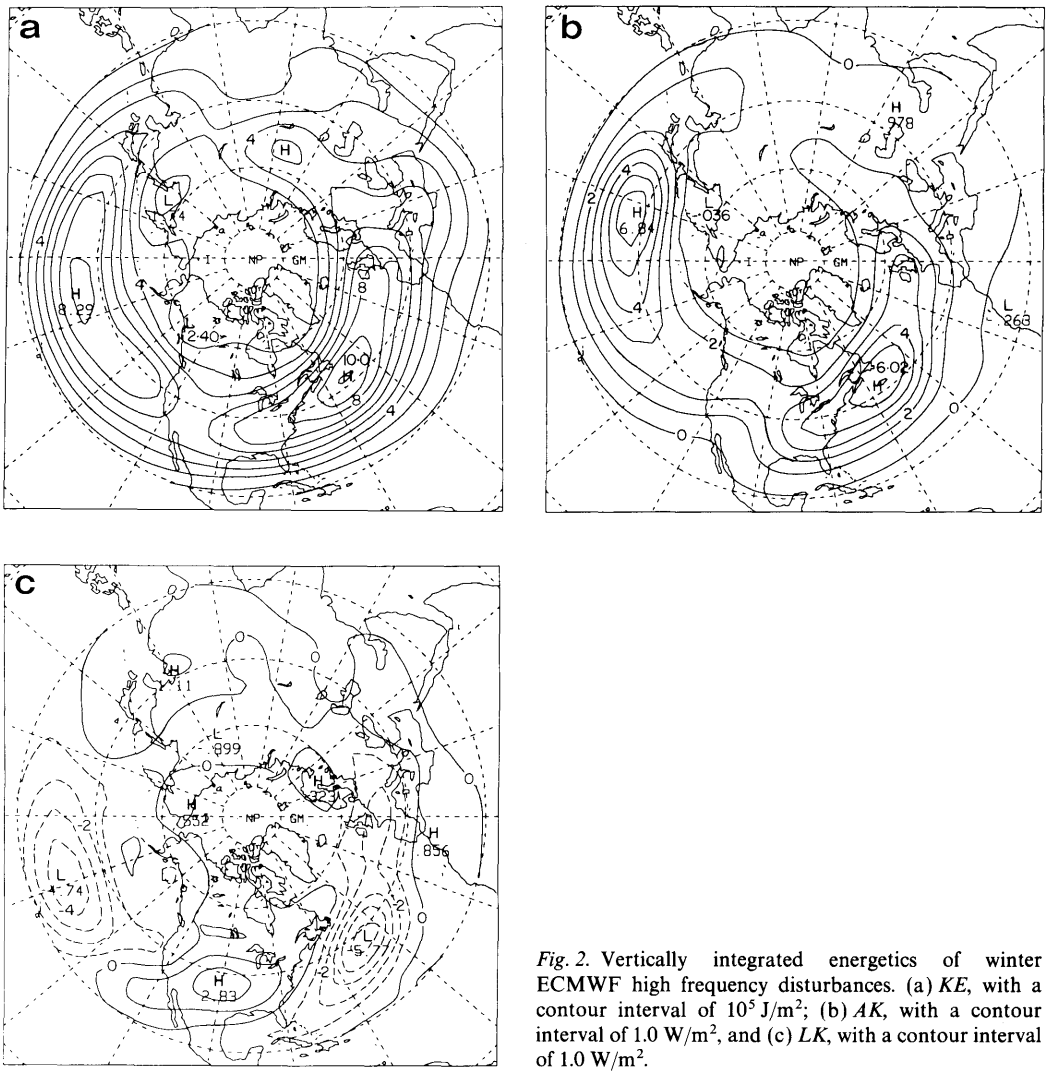

Fig. 2. Vertically integrated energetics of winter ECMWF high frequency disturbances. (a) *KE*, with a contour interval of 10^5 J/m^2; (b) *AK*, with a contour interval of 1.0 W/m^2, and (c) *LK*, with a contour interval of 1.0 W/m^2.

much weaker, can be found east of the Urals. The Tibetan Plateau and the Rockies, which separate the Atlantic and Pacific maxima, are noted to have low values of *KE*. These features are consistent with the results documented in Blackmon et al. (1977), in which 2.5–6 day high-pass filtered geopotential heights at 500 mb were used to characterize the fast transients. One notable difference is that the center near the Urals was much stronger in Blackmon et al.'s (1977) geopotential analyses.

The distribution of available potential energy for the fast transients (not shown) is very similar to that of kinetic energy. The high frequency maxima are located over the western Atlantic and Pacific regions, somewhat westward of the fast transient *KE* maxima. The third maximum east of the Urals is, however, less visible in the *APE* map. The similarity among the patterns of *KE*, *APE* and the baroclinic conversion term, *AK* (Fig. 2b), in the high frequency range is remarkable. The winter stationary waves tend to organize baroclinic eddies in elongated storm tracks without dramatically changing their essential wave structure,

evolution and energetics. In a linear baroclinic stability analysis of the longitudinally dependent climatological mean flow, Frederiksen (1983a, b) was able to simulate the observed fact that the fastest growing baroclinic wave modes exhibit their largest amplitudes in the strom track regions. Hoskins (1983) also discussed the role of the time-mean flow in maintaining the storm track structure. The high-frequency energetics shown in Fig. 2a and b are consistent with the energy cycle suggested by baroclinic instability theory, but modified by the fact that the growth of the disturbances is modulated by the presence of the stationary planetary waves.

The barotropic exchange of *KE* between the time-mean flow and the fast transients, *LK*, also shows well-defined patterns (Fig. 2c). The synoptic scale eddies lose *KE* mainly in the western Atlantic and eastern Pacific. In the Atlantic region, the maximum energy loss is located slightly east of the maximum center of *KE*, while its Pacific counterpart is near 160° W and 30° N. A positive conversion (mean flow to transients) is found over the North American continent. The entire Eurasia and west Pacific show signs of weak but positive values. The patterns are very similar to those of Wallace and Lau (1985), except that the present center in the Pacific is about 20° further east.

The modeling study by Simmons and Hoskins (1978) on the time evolution of nonlinear transient disturbances illustrates the life cycle of synoptic eddies. Baroclinic waves superimposed on a balanced zonal mean flow are seen to grow initially by baroclinic instability with a vigorous generation of eddy *APE* and *KE*. After about a week of model simulation, these disturbances reach the occluded stage and become more nearly barotropic, with a correspondingly much weakened heat flux. As the waves propagate further eastward, the structure of the momentum fluxes generally results in the transfer of *KE* from the transient eddies to the mean flow. Observations reveal that in the atmosphere, eastern Asia and eastern North America are found to have strong vertical wind shears and therefore are propitious sites for the initiation of baroclinic development of synoptic scale cyclones. As the disturbances move along the storm tracks they gradually acquire a barotropic structure. In terms of the energetics of the high frequency transients discussed in this section, the theoretical and modeling results seem capable of providing a sound framework to explain the geographical distributions of the energy conversion terms.

Fig. 3a shows the distribution of kinetic energy during the winter for transients with periods longer than 10 days. The salient features are the

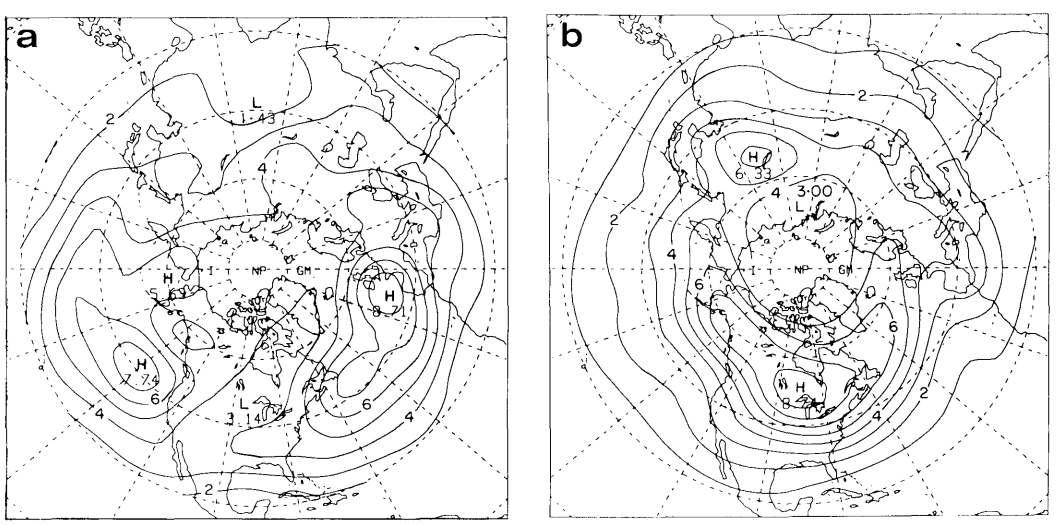

Fig. 3. Vertically integrated energetics of winter ECMWF low frequency disturbances. (a) *KE*, with a contour interval of 10^5 J/m^2; (b) *APE*, with a contour interval of 10^5 J/m^2; (c) *AK*, with a contour interval of 0.5 W/m^2; (d) *LK*, with a contour interval of 1.0 W/m^2; (e) *BT*, with a contour interval of 0.5 W/m^2 and (f) *NK*, with a contour interval of 1.0 W/m^2.

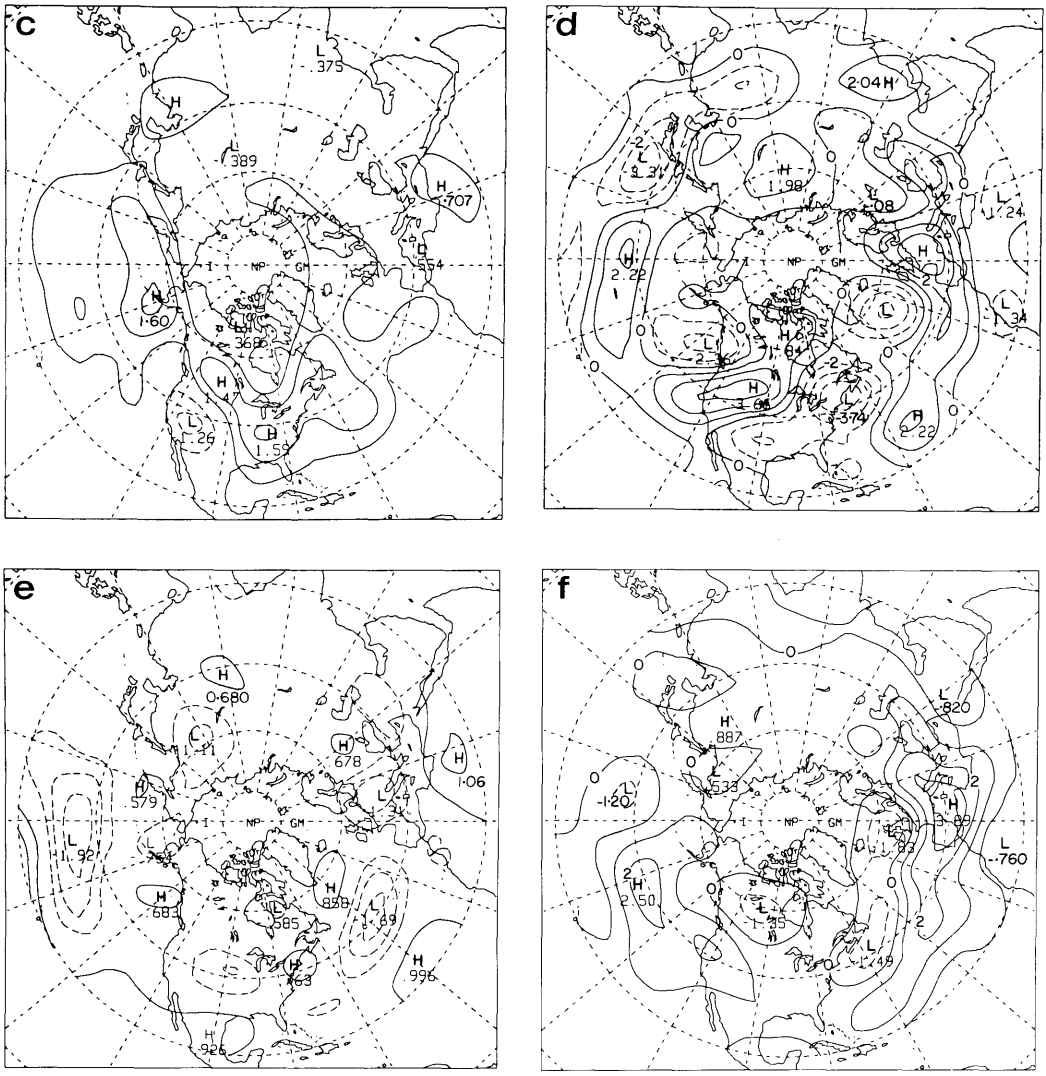

Fig. 3 (continued)

two maxima over the eastern oceans, which are less elongated in the east-west direction than those of the fast transients (Fig. 2a). They are located to the east of the high frequency maxima and at somewhat higher latitudes (about 5°). In comparison with the maxima of low frequency variance derived from the 500 mb height field, these centers of transient activity are located further eastward and at slightly lower latitudes (see Blackmon et al., 1977). It is also noted that the third maximum over the Siberian arctic, usually appearing in the variance of the 500 mb geopotential height, is hardly detected in the present *KE* analysis. These preferred locations of low frequency activity appear to be related to regions of frequent blocking, identified by Rex (1950) and documented more recently by Dole (1986). The regions of minimum slow transient activity, as in the case of the fast transients, are found over the Tibetan Plateau and the Rockies.

The geographical distribution of the low frequency *APE* (Fig. 3b) is fundamentally different

from that of *KE*. The two major maxima are located over North America and eastern Mongolia. No strong centers can be found in either the Atlantic or the Pacific region. Unlike their high-frequency counterparts, the wind disturbances of slow transients are associated with no significant temperature perturbations, which is another way of stating that the low-frequency eddies have a barotropic or quasi-barotropic structure, as found by Blackmon et al. (1979). The latter showed that over the eastern oceans the low-frequency fluctuations of geopotential height exhibit a barotropic structure, whereas the continental regions to the north and east of the Rockies and Himalayas are notable for their more baroclinic structure. The present results are consistent with these findings.

The geographical distribution of the integrand appearing in AK, the baroclinic energy conversion, is shown in Fig. 3c for the low-frequency disturbances. The main maxima are located over North America, the east coast of Asia, and the northern Pacific ocean. It is of interest to note that AK is either negative or weakly positive over the eastern oceans, where the kinetic energy of the slow transients is strongest. The results presented in Sheng and Hayashi (1990a, b) and in Section 3 of this paper all indicate that, for area-integrated quantities, the baroclinic conversion is the major energy source for the low frequency eddies. This is true not only during the winter but also in the annual mean sense. It is interesting to note that the main contributions to the integrand appearing in AK' do not come from the eastern oceanic regions. The lack of contribution from the baroclinic energy conversion in the regions of strong low frequency *KE* is in agreement with the quasi-barotropic structure found by Blackmon et al. (1979).

The barotropic *KE* conversion term LK' is illustrated in Fig. 3d. Positive centers are located over the west coasts of North America and Europe, extending towards the southwest direction. Negative values of LK' are found in the western parts of the Atlantic and Pacific, where the low frequency *KE* is relatively weak. By comparison with the baroclinic conversion AK', the barotropic term apparently shows a better correspondence with the kinetic energy in terms of the geographic distributions. The barotropic *KE* conversion from the slow transients to the time-mean flow, BT' (see Appendix A for its expression) is shown in Fig. 3e, which sharply contrasts with the results displayed in Fig. 3d. It is stressed that due to the existence of a mean flow transport of transient *KE*, the local energy gain by the transients LK does not equal the local energy loss by the mean flow shown in Fig. 3e (cf. Appendix A). The most significant features are two negative centers in the mid-oceans where the time-mean flow loses kinetic energy to the transient eddies. It is noted that the regions of strong *KE* conversion are located downstream of the jet-stream exit, suggesting that, as proposed by Hoskins et al. (1983), the low frequency transients, elongated in the east-west direction, produce a westward $\boldsymbol{E}$ vector (Wallace and Lau, 1985). This implies a down-gradient flux of momentum and a transfer of *KE* from the mean flow to the slow transients. The distribution shown in Fig. 3e is consistent with the notion that the mean flow supplies *KE* to the slow transients in the mid-oceans by the mechanism of a down-gradient flux of momentum (not shown).

The gain of kinetic energy by the slow transients due to the nonlinear interactions with the fast transient eddies, NK', is shown in Fig. 3f. It is very interesting to observe some similarities between the patterns shown in Figs. 3d and 3f. Once again, positive regions are present in the eastern regions of the Atlantic and Pacific. Due to the smaller negative contributions from the western oceans, the net conversion from NK' is much greater than LK' when averaged over the entire Northern Hemisphere, as was discussed in Section 3.

Frederiksen (1983b) conducted a linear stability analysis of a three-dimensional model with a realistic winter mean state. A variety of unstable modes were obtained, including propagating cyclogenetic modes, onset-of-blocking modes and low frequency "teleconnection" modes. It was found that, for an increasingly larger static stability parameter, the fastest growing model modes assume a structure that is more and more barotropic. Nevertheless, the baroclinic energy conversion did enhance the growth rate of the unstable modes, even at very low frequencies. In the present hemispherically averaged energetics, it is found that during winter the main sources of low-frequency *KE* (Fig. 1a) are the baroclinic conversion and the transfer of *KE* from the fast transients. While smaller by a factor of about 3, the transfer of *KE* from the time mean flow to the slow transients is still of local importance.

The current understanding of the relationship between the low frequency variability and the theory of barotropic instability is based, to a large extent, upon the studies by Simmons et al. (1983) and Wallace and Lau (1985). These studies have provided ample evidence of the barotropic extraction of kinetic energy by the slow transients from the winter climatological mean flow. More recently, Nakamura et al. (1987) demonstrated that five typical teleconnection patterns are all associated with an energy conversion in the sense described above. The Pacific/North American and Eastern Atlantic patterns were found to have the largest conversions by far, due to the fact that these patterns have "seesaws" located in the jet-exit regions and therefore obtain *KE* more effectively than the other patterns. The evidence presented in Figs. 3d and 3e indicates that *KE* is extracted from the jet-exit regions and supplied to the low frequency transients further downstream. Therefore, the notion of barotropic energy conversion from the time-mean flow to the eddies and the barotropic instability due to the zonal and meridional variations of the mean flow are still valid even for a baroclinic basic state.

The transfer of *KE* to the low frequency transients from high-frequency baroclinic waves (Fig. 3f) exhibits a horizontal distribution which is similar to the barotropic term (Fig. 3d). This suggests that the slow transients are organized by the winter stationary waves in such a way as to extract *KE* from not only the mean flow but also from the synoptic scale eddies in the eastern regions of the major oceans. Barotropic instability and forcing by the high frequency transients function coherently to enhance the low frequency transients. It would seem that the low-frequency regime, in some sense, should be considered as a barotropically unstable system forced by the fast transients, instead of a barotropically free unstable system. This is consistent with the results of Mullen (1987), Holopainen and Fortelius (1987), and Lau (1988) who examined the relationship between the slowly varying part of the flow and the fast baroclinic waves. They found that the latter tend to reinforce the time fluctuations present in the former. According to the calculations shown in Section 3 and the present section, nonlinear interactions provide much more *KE* to the winter slow transients than does the barotropic exchange with the time-mean flow. They are therefore of importance both locally and hemispherically for the energy balance of the low frequency regime. At this stage, little is known about the structure and evolution of the low frequency momentum and thermal forcings due to the nonlinear interactions with the high-frequency eddies. Shutts (1983) did, however, conduct numerical simulations of eddy forcing during a blocking episode, which provided the basis for a qualitative understanding of the process.

5. Local contributions to the summertime energetics

It was demonstrated in Section 3 that the energy cycle experiences strong seasonal oscillations in all the frequency bands discussed, with the *APE* and *KE* levels showing consistently higher values in the winter season. The energy conversion terms undergo more complicated evolutions, a significant example being the reversal of the barotropic conversion of *KE* for the low frequency transients. In this section, the energetics of the summer season are further studied in terms of local contributions to the hemispheric integrals.

The distribution of kinetic energy is shown in Fig. 4a for the high frequency transients. A comparison with Fig. 2a reveals that the geographic patterns of *KE* are similar for the winter and the summer seasons. The storm tracks are still located over the Atlantic and Pacific oceans, but at somewhat higher latitudes, in agreement with the modelling results of Frederiksen (1983a). The strength of the storm activity is considerably reduced, especially in the Atlantic region. It is also noted that the storm tracks are less elongated in the zonal direction when compared with their counterparts in the winter season. Other features, such as the third maximum east of the Urals and the relatively low values near the Rockies and the Tibetan Plateau, can still be detected but are less significant. As in the winter season, the distribution of available potential energy for the fast transients (not shown) is similar to that of kinetic energy. The elongated maxima are clearly related to the storm tracks, but shifted westward. These are indications that high frequency transients are baroclinic disturbances, as in the winter season. Fig. 4b shows the pattern of baroclinic conversion, AK', which shares a clear resemblance with those

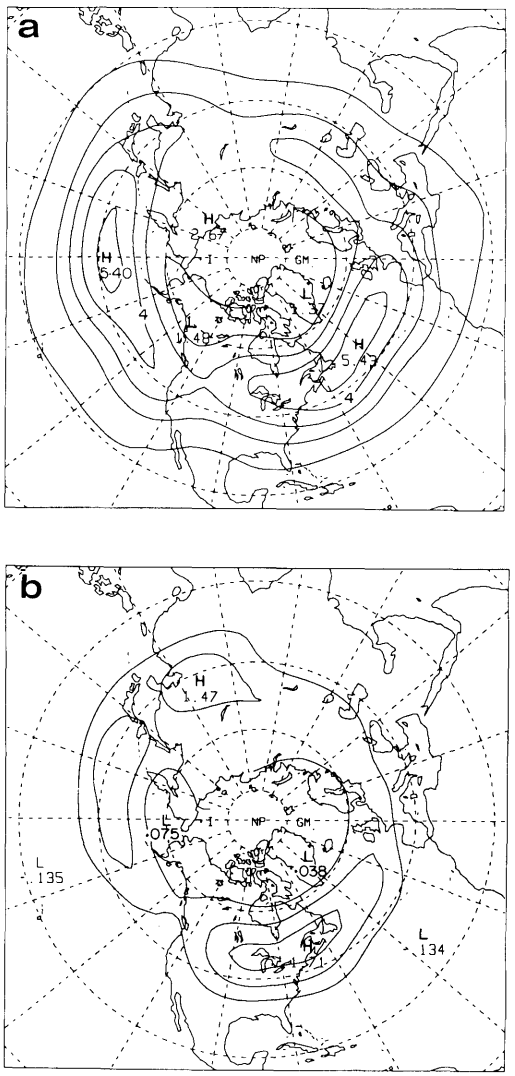

Fig. 4. Vertically integrated energetics of summer ECMWF high frequency disturbances. (a) KE, with a contour interval of 10^5 J/m^2 and (b) AK, with a contour interval of 0.5 W/m^2.

of KE and APE. In view of the present results, it is concluded that the high frequency eddies still owe their origin to the baroclinic instability of the three dimensional flow, although the baroclinicity of the summer mean state is much weaker than that of the winter.

It comes as no surprise that the local energy balance of the fast transients found during summer is very similar to that in winter, as can be expected from the similarity of the hemispherically integrated energy cycles for the summer and winter seasons. It is found, however, that similarities also exist in the energy balance of the slow transients, even though the role of the barotropic energy conversion is reversed for the two seasons.

Fig. 5a shows the geographical distribution of kinetic energy for the slow transients. The centers of maximum activity are located significantly eastward of the positions of the summer storm tracks. The energy level of maximum KE is diminished considerably in comparison with the winter. Fig. 5b is the same as Fig. 5a, but for the available potential energy. Two maxima can be found in the continental regions of northern Canada and western Siberia, which are completely out of phase with the active regions of low frequency wind variability. By the same argument as that presented in Section 4, the lack of association between KE and APE is consistent with the quasi-barotropic structure of the low frequency transients as discussed in Blackmon et al. (1979).

The local baroclinic energy conversion AK is shown in Fig. 5c for the slow transients. The major centers are found in Canada and east China

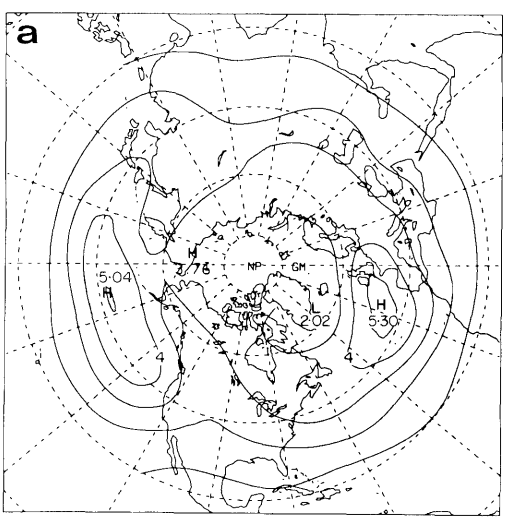

Fig. 5. Vertically integrated energetics of summer ECMWF low-frequency disturbances. (a) KE, with a contour interval of 10^5 J/m^2, (b) APE, with a contour interval of 10^5 J/m^2, (c) AK, with a contour interval of 0.5 W/m^2, (d) LK, with a contour interval of 0.5 W/m^2 and (e) $LK + NK$, with a contour interval of 0.5 W/m^2.

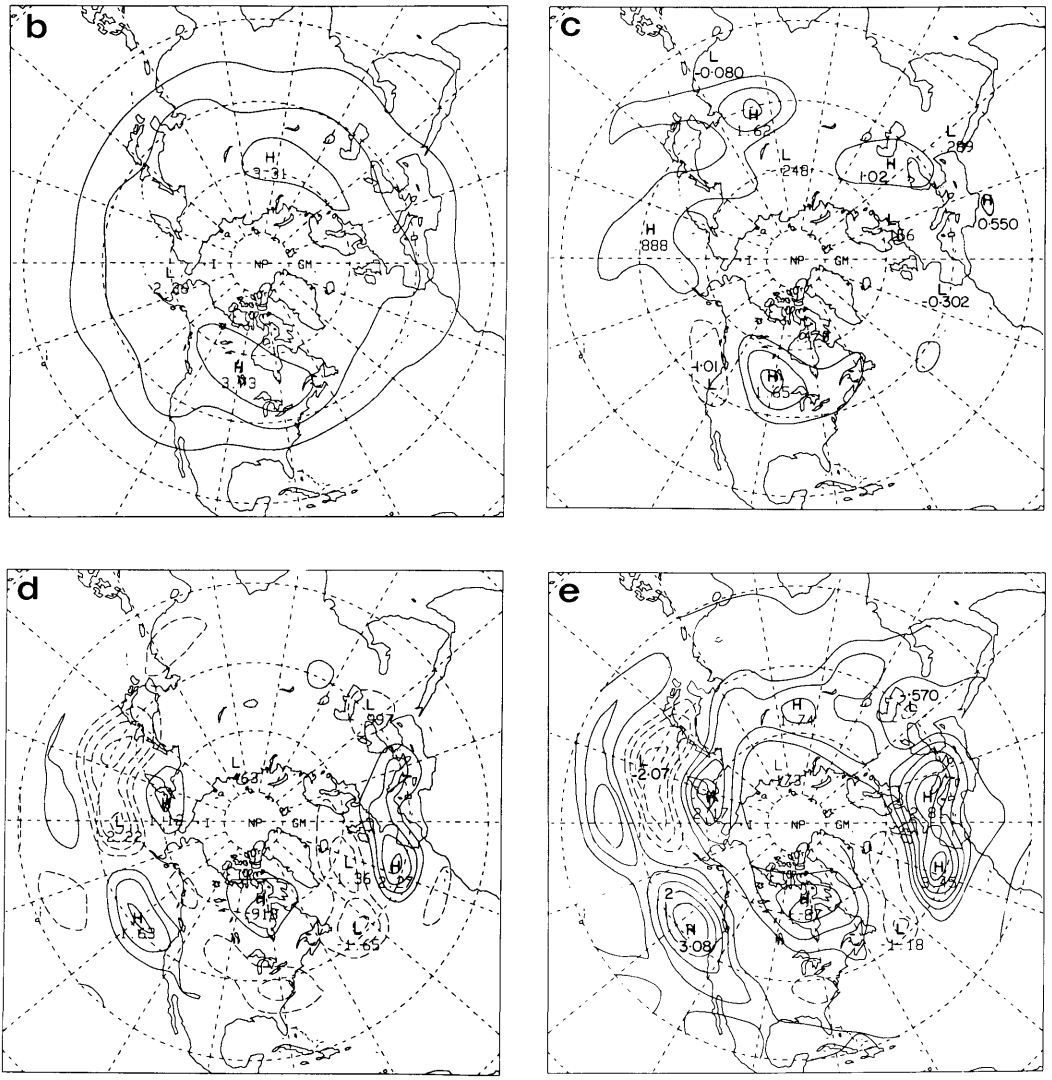

Fig. 5 (continued)

extending to the western Pacific. No significant baroclinic conversion is found in the regions of strong low frequency *KE*, as was also observed for the winter case. It is evident that the baroclinic energy conversion is hindered by the quasi-barotropic structure of the slow transients. LK^{ℓ}, the barotropic conversion of *KE*, is presented in Fig. 5d. In much the same way as in the winter season, the stationary waves serve to supply *KE* and organize the transient activity in the eastern regions of the Atlantic and Pacific oceans. However, negative conversions are found over the western regions of the oceans, which results in a net transfer of *KE* from the eddies to the mean flow in a hemispheric integration (Fig. 1b). Again, the dipole appearance of the patterns in Fig. 5d suggests that the advective part of the expression for LK^{ℓ} is locally dominant, although it does not contribute to the hemispheric average. The negative value obtained for the hemispherically

averaged LK^{ℓ} (Fig. 1b) indicates that the summer stationary waves are not sufficiently strong to support the mechanism of barotropic instability proposed by Simmons et al. (1983). Fig. 5e shows the contribution from the sum of LK^{ℓ} and NK^{ℓ}, which possesses many features of LK^{ℓ}. It is therefore suggested that, in a sense, the interactions with the synoptic scale eddies act as a forcing on a barotropically stable mean state, which arranges the sites for the activity of the slow transients.

6. Conclusions

In the present study, spectral energetics in the frequency domain have been calculated using the ECMWF operational analyses separately for the winter and summer seasons, with the following conclusions being of interest.

(i) The atmospheric energetics in the frequency domain undergo a seasonal cycle such that the annual variation is stronger in the high frequency band than in the low frequency band. Generally, the levels of energy and energy conversion terms are both higher during the winter, as would be expected. When integrated over the Northern Hemisphere, the baroclinic conversion is the primary *KE* source for both winter and summer seasons for the three frequency groups considered. For the low-frequency transients, the nonlinear exchange of kinetic energy, i.e., the energy supplied by the synoptic scale disturbances, is also important. The barotropic conversion of kinetic energy (between the time-mean flow and the low frequency transients) changes sign from the cold to the warm season. The climatological mean flow appears to be barotropically unstable during winter but stable during the summer.

(ii) The geographical distributions of *KE* and *APE* for different frequency bands indicate that high frequency disturbances are organized by the time-mean flow into storm tracks and that the low frequency disturbances are most active further eastward where the phenomenon of blocking frequently occurs. One important observation is that the slow transients have predominantly a quasi-barotropic structure, which is indicated by the separation of the centers of *KE* and *APE*.

(iii) In both the winter and summer seasons, the distributions of energy and energy conversion terms for the synoptic scale eddies are in good agreement with the classical theory of baroclinic instability modified by the presence of stationary waves. The fast transients are observed to be baroclinically unstable and barotropically stable.

(iv) The baroclinic conversion for the slow transients is weak in the eastern regions of the Atlantic and Pacific oceans where the level of low-frequency *KE* is high. Although the domain-integrated value of the barotropic conversion is negative during the summer, its spatial distribution is in many ways similar to that found for the winter. It is of great interest that the nonlinear and barotropic conversions of *KE* appear to reinforce each other and enhance the low-frequency activity in the eastern regions of the major oceans. The present results suggest that, during the winter, the low-frequency disturbances over the oceans can be viewed as modes that are forced by the fast baroclinic eddies and grow in a barotropically unstable, zonally varying basic state. Over land the low-frequency eddies seem to grow baroclinically.

The spectral energetics studied in Sheng and Hayashi (1990a, b), using data sets taken from observations during the FGGE year and simulations at GFDL, demonstrated that the kinetic energy of the low frequency transients is primarily maintained by the conversion from the available potential energy. Schubert (1986) found that the net barotropic and baroclinic conversions were of comparable magnitudes for periods greater than 10 days while the baroclinic conversion dominates for shorter periods. The study of Wallace and Lau (1985), using observational and GCM data sets, confirmed that the barotropic energy conversion is an important energy source for the slow transients during the winter. Nakamura et al. (1987) have also shown that the major teleconnection patterns are structured to extract *KE* from the zonally varying climatological mean flow. From the results presented above, the energy balance of the slow transients appears more complicated than was previously thought. Although the baroclinic conversion is the major energy source for the Northern Hemisphere as a whole, the barotropic and nonlinear conversions provide the main features of the local energy balance over the eastern areas of the Atlantic and Pacific. Moreover, the nonlinear effects are even more important in the summer season since, in a hemispherically averaged sense, the mechanism of barotropic instability supplies no net energy to the disturbances.

The limitations of the ECMWF data set should be properly addressed. It is well-known that the ECMWF analyses systematically underestimate the divergent component of the wind field, mainly in the tropics. The energy cycles during the FGGE year, computed from the ECMWF and GFDL data sets show considerable discrepancy in the spectral estimates of the baroclinic energy conversion, although general agreement was found on the directions and magnitudes of the energy flow (Sheng and Hayashi, 1990a). In particular, the ECMWF data yield a smaller baroclinic conversion than the GFDL data. The geographical distributions of the baroclinic energy conversions are therefore subject to some uncertainty and caution should be exercised in their interpretation. However, since only maps of the extratropical region (north of 20° N) have been shown, this problem sould not seriously affect the main conclusions of the present study.

Finally, it should be realized that the results presented in the present study apply to the average behavior of the atmosphere over the period considered. It is quite conceivable that during subperiods the behavior may be quite different. For example, energy transfers taking place during the life cycle of an atmospheric blocking event, as in the case studied by Holopainen and Fortelius (1987), need not be the same as those presented here. Nevertheless, it is of interest to document the average features of the atmosphere. In addition to being of interest by themselves, the results may be quite useful in evaluating the performance of general circulation models.

7. Acknowledgements

The authors would like to acknowledge the financial support of the Natural Sciences and Engineering Research Council of Canada, the Atmospheric Environment Service of Canada and McGill University. They would also like to thank Ms. U. Seidenfuss for her help with some of the diagrams.

8. Appendix A

Spectral energy equations for KE and APE

The derivations of the spectral energy equations in the frequency domain were presented in Sheng (1986) and Sheng and Hayashi (1990a). The equations of *KE* and *APE* for the low- and high-frequency bands can be written as,

$$LK^{\ell} + NK^{\ell} + AK^{\ell} + FK^{\ell} + FP^{\ell} - D^{\ell} = 0,$$

$$LK^{\mathrm{h}} + NK^{\mathrm{h}} + AK^{\mathrm{h}} + FK^{\mathrm{h}} + FP^{\mathrm{h}} - D^{\mathrm{h}} = 0,$$

$$LA^{\ell} + NA^{\ell} - AK^{\ell} + FA^{\ell} + G^{\ell} = 0,$$

$$LA^{\mathrm{h}} + NA^{\mathrm{h}} - AK^{\mathrm{h}} + FA^{\mathrm{h}} + G^{\mathrm{h}} = 0.$$

Here the superscripts ℓ and h denote the energy transfer terms for the low- and high-frequency bands, respectively. The mathematical expression for each term is given in the following:

$$LK^{\ell} = -\overline{u_{\ell}\left[\nabla\cdot(\bar{u}\boldsymbol{V}_{\ell} + u_{\ell}\bar{\boldsymbol{V}}) - \frac{\tan\phi}{a}(\bar{u}v_{\ell} + u_{\ell}\bar{v})\right]}$$
$$-\overline{v_{\ell}\left[\nabla\cdot(\bar{v}\boldsymbol{V}_{\ell} + v_{\ell}\bar{\boldsymbol{V}}) + \frac{\tan\phi}{a}(\bar{u}u_{\ell} + u_{\ell}\bar{u})\right]},$$

$$LK^{\mathrm{h}} = -\overline{u_{\mathrm{h}}\left[\nabla\cdot(\bar{u}\boldsymbol{V}_{\mathrm{h}} + u_{\mathrm{h}}\bar{\boldsymbol{V}}) - \frac{\tan\phi}{a}(\bar{u}v_{\mathrm{h}} + u_{\mathrm{h}}\bar{v})\right]}$$
$$-\overline{v_{\mathrm{h}}\left[\nabla\cdot(\bar{v}\boldsymbol{V}_{\mathrm{h}} + v_{\mathrm{h}}\bar{\boldsymbol{V}}) + \frac{\tan\phi}{a}(\bar{u}u_{\mathrm{h}} + u_{\mathrm{h}}\bar{u})\right]},$$

$$NK^{\ell} = -\overline{u_{\ell}\left[\nabla\cdot(u_{\ell}\boldsymbol{V}_{\mathrm{h}} + u_{\mathrm{h}}\boldsymbol{V}_{\ell} + u_{\mathrm{h}}\boldsymbol{V}_{\mathrm{h}})\right.}$$
$$\left.-\frac{\tan\phi}{a}(u_{\ell}v_{\mathrm{h}} + u_{\mathrm{h}}v_{\ell} + u_{\mathrm{h}}v_{\mathrm{h}})\right]_{\ell}$$
$$-\overline{v_{\ell}\left[\nabla\cdot(v_{\ell}\boldsymbol{V}_{\mathrm{h}} + v_{\mathrm{h}}\boldsymbol{V}_{\ell} + v_{\mathrm{h}}\boldsymbol{V}_{\mathrm{h}})\right.}$$
$$\left.+\frac{\tan\phi}{a}(u_{\ell}u_{\mathrm{h}} + u_{\mathrm{h}}u_{\ell} + u_{\mathrm{h}}u_{\mathrm{h}})\right]_{\ell},$$

$$NK^{\mathrm{h}} = -\overline{u_{\mathrm{h}}\left[\nabla\cdot(u_{\ell}\boldsymbol{V}_{\mathrm{h}} + u_{\mathrm{h}}\boldsymbol{V}_{\ell} + u_{\ell}\boldsymbol{V}_{\ell})\right.}$$
$$\left.-\frac{\tan\phi}{a}(u_{\ell}v_{\mathrm{h}} + u_{\mathrm{h}}v_{\ell} + u_{\ell}v_{\ell})\right]_{\mathrm{h}}$$
$$-\overline{v_{\mathrm{h}}\left[\nabla\cdot(v_{\ell}\boldsymbol{V}_{\mathrm{h}} + v_{\mathrm{h}}\boldsymbol{V}_{\ell} + v_{\ell}\boldsymbol{V}_{\ell})\right.}$$
$$\left.+\frac{\tan\phi}{a}(u_{\ell}u_{\mathrm{h}} + u_{\mathrm{h}}u_{\ell} + u_{\ell}u_{\ell})\right]_{\mathrm{h}},$$

$$FK^{\ell} = -\nabla \cdot \overline{[\tfrac{1}{2}(u_{\ell}^2 + v_{\ell}^2)\, V_{\ell}]},$$

$$FK^{\mathrm{h}} = -\nabla \cdot \overline{[\tfrac{1}{2}(u_{\mathrm{h}}^2 + v_{\mathrm{h}}^2)\, V_{\mathrm{h}}]},$$

$$FP^{\ell} = -\nabla \cdot \overline{(\phi_{\ell} V_{\ell})},$$

$$FP^{\mathrm{h}} = -\nabla \cdot \overline{(\phi_{\mathrm{h}} V_{\mathrm{h}})},$$

$$D^{\ell} = -\overline{(u_{\ell} F_{u\ell} + v_{\ell} F_{v\ell})},$$

$$D^{\mathrm{h}} = -\overline{(u_{\mathrm{h}} F_{u\mathrm{h}} + v_{\mathrm{h}} F_{v\mathrm{h}})},$$

$$AK^{\ell} = -\overline{\omega_{\ell} \alpha_{\ell}},$$

$$AK^{\mathrm{h}} = -\overline{\omega_{\mathrm{h}} \alpha_{\mathrm{h}}},$$

$$LA^{\ell} = -\gamma \overline{\theta_{\ell}^* \nabla \cdot (\theta_{\ell}^* \bar{V} + \bar{\theta}^* V_{\ell})},$$

$$LA^{\mathrm{h}} = -\gamma \overline{\theta_{\mathrm{h}}^* \nabla \cdot (\theta_{\mathrm{h}}^* \bar{V} + \bar{\theta}^* V_{\mathrm{h}})},$$

$$NA^{\ell} = -\gamma \overline{\theta_{\ell}^* \nabla \cdot (\theta_{\ell}^* V_{\mathrm{h}} + \theta_{\mathrm{h}}^* V_{\ell} + \theta_{\mathrm{h}}^* V_{\mathrm{h}})_{\ell}},$$

$$NA^{\mathrm{h}} = -\gamma \overline{\theta_{\mathrm{h}}^* \nabla \cdot (\theta_{\ell}^* V_{\mathrm{h}} + \theta_{\mathrm{h}}^* V_{\ell} + \theta_{\ell}^* V_{\ell})_{\mathrm{h}}},$$

$$FA^{\ell} = -\gamma \nabla \cdot \overline{(\tfrac{1}{2}\theta_{\ell}^{*2} V_{\ell})},$$

$$FA^{\mathrm{h}} = -\gamma \nabla \cdot \overline{(\tfrac{1}{2}\theta_{\mathrm{h}}^{*2} V_{\mathrm{h}})},$$

$$G^{\ell} = \gamma \left(\frac{\theta}{C_{\mathrm{p}} T}\right) \overline{\theta_{\ell}^* Q_{\ell}^*},$$

$$G^{\mathrm{h}} = \gamma \left(\frac{\theta}{C_{\mathrm{p}} T}\right) \overline{\theta_{\mathrm{h}}^* Q_{\mathrm{h}}^*}.$$

In the above equations, each time series has been decomposed into the time-mean, the low-frequency and the high-frequency parts,

$$f = \bar{f} + f_{\ell} + f_{\mathrm{h}}.$$

A list of symbols, definitions and variables are given in Appendix B. The expression for the barotropic conversion, LK, represents the kinetic energy locally transferred into the transient eddies. Figs. 2c and 3d illustrate the geographical distribution of this term for the high- and the low-frequency bands, respectively. On the other hand, an alternate equation for the barotropic conversion can be derived by mass averaging LK over a closed domain and performing an integration by parts, to obtain

$$\{BT^{\ell}\} = -\{LK^{\ell}\}$$

$$= \left\{ \overline{u_{\ell} V_{\ell}} \cdot \nabla \bar{u} + \overline{v_{\ell} V_{\ell}} \cdot \nabla \bar{v} + \frac{\tan \phi}{a} \left[\overline{u_{\ell} v_{\ell}}\, \bar{u} - \overline{u_{\ell} u_{\ell}}\, \bar{v} \right] \right\},$$

$$\{BT^{\mathrm{h}}\} = -\{LK^{\mathrm{h}}\}$$

$$= \left\{ \overline{u_{\mathrm{h}} V_{\mathrm{h}}} \cdot \nabla \bar{u} + \overline{v_{\mathrm{h}} V_{\mathrm{h}}} \cdot \nabla \bar{v} + \frac{\tan \phi}{a} \left[\overline{u_{\mathrm{h}} v_{\mathrm{h}}}\, \bar{u} - \overline{u_{\mathrm{h}} u_{\mathrm{h}}}\, \bar{v} \right] \right\}.$$

Here $\{f\}$ represents the mass average of the function f. The integrand of the above expression for BT is shown in Fig. 3e for the low-frequency band. It is seen that, when integrated over a closed domain, LK is identical to BT but with the opposite sign. The local difference between the two expressions is due to the transport of transient KE by the time-mean flow (Hayashi, 1980), which vanishes upon integration over the mass of the atmosphere. Wallace and Lau (1985) essentially applied the formula for BT, with some simplifications, to their single level data sets to calculate the barotropic KE conversion.

Appendix B

List of symbols

a	earth's radius
C_{p}	specific heat at constant pressure
F_u	frictional force in the x-direction
F_v	frictional force in the y-direction
g	force of gravity per unit mass
p	pressure
Q	diabatic heating
T	temperature
u	eastward component of velocity
v	northward component of velocity
V	three-dimensional velocity vector
z	geopotential height
α	specific volume
γ	static stability parameter
θ	potential temperature
ϕ	latitude
ω	vertical pressure velocity
$\overline{(\ )}$	time average
$\{(\ )\}$	mass average
$(\ )^*$	deviation from the horizontal mean
$(\ )_{\mathrm{h}}$	high frequency component of a time series
$(\ )^{\mathrm{h}}$	energy transfer term for the high-frequency band
$(\ )_{\ell}$	low frequency component of a time series

$( )'$ energy transfer term for the low-frequency band
∇ three-dimensional gradient operator
AK baroclinic conversion from APE to KE
D dissipation of transient KE
FA convergence of transient APE flux
FK convergence of transient KE flux
FP convergence of transient flux of potential energy
G generation of transient APE
LA transfer of APE from the time-mean flow to the transient eddies
LK transfer of KE from the time-mean flow to the transient eddies
NA transfer of APE due to nonlinear interactions of transient eddies
NK transfer of KE due to nonlinear interactions of transient eddies
BT an alternate expression for barotropic energy conversion

REFERENCES

Blackmon, M. L., Wallace, J. M., Lau, N.-C. and Mullen, S. L. 1977. An observational study of the Northern Hemisphere wintertime circulation. *J. Atmos. Sci. 34*, 1040–1053.

Blackmon, M. L., Madden, R. A., Wallace, J. M. and Gutzler, D. S. 1979. Geographical variations in the vertical structure of geopotential height fluctuations. *J. Atmos. Sci. 36*, 2450–2466.

Charney, J. G. 1947. The dynamics of longwaves in a baroclinic westerly current. *J. Meteor. 4*, 135–163.

Chen, T. C. and Wiin-Nielsen, A. 1978. On nonlinear cascades of atmospheric energy and enstrophy in a two dimensional spectral index. *Tellus 30*, 313–322.

Dole, R. M. 1986. Persistent anomalies of the extratropical Northern Hemisphere wintertime circulation: Structure. *Mon. Wea. Rev. 114*, 178–207.

Eady, E. T. 1949. Long waves and cyclone waves. *Tellus 1*, 33–52.

Frederiksen, J. S. 1983a. Disturbance and eddy fluxes in Northern Hemisphere flows: Instability of three-dimensional January and July flows. *J. Atmos. Sci. 40*, 836–855.

Frederiksen, J. S. 1983b. A unified three-dimensional instability theory of the onset of blocking and cyclogenesis. II: Teleconnection patterns. *J. Atmos. Sci. 40*, 2593–2609.

Hayashi, Y. 1980. Estimation of nonlinear energy transfer spectra by the cross-spectral method. *J. Atmos. Sci. 37*, 299–307.

Holopainen, E. and Fortelius, C. 1987. High frequency eddies and blocking. *J. Atmos. Sci. 44*, 1632–1645.

Hoskins, B. J. 1983. Modelling of the transient eddies and their feedback on the mean flow. In: *Large-scale dynamical processes in the atmosphere*, (eds. B. J. Hoskins and R. P. Pearce). Academic Press, New York, 169–199.

Hoskins, B. J., James, I. N. and White, G. H. 1983. The shape, propagation and mean-flow interaction of large scale weather systems. *J. Atmos. Sci. 40*, 1595–1612.

Kuo, H.-L. 1949. Dynamical instability of two dimensional nondivergent flow in a barotropic atmosphere. *J. Meteor. 6*, 105–122.

Lau, N.-C. 1988. Variability of the observed midlatitude cyclone tracks in relation to low-frequency changes in the circulation pattern. *J. Atmos. Sci. 45*, 2718–2743.

Lorenz, E. N. 1967. The Nature and Theory of the General Circulation of the atmosphere. World Meteorological Organization, Geneva, Switzerland, 161 pp.

Mullen, S. L. 1987. Transient eddy forcing of blocking flows. *J. Atmos. Sci. 44*, 3–22.

Nakamura, H. Tanaka, M. and Wallace, J. M. 1987. Horizontal structure and energetics of Northern Hemisphere wintertime teleconnection patterns. *J. Atmos. Sci. 44*, 3377–3391.

O'Brien, J. J. 1970. Alternative solutions to the classical vertical velocity problem. *J. Appl. Meteor. 9*, 197–203.

Rex, D. F. 1950. Blocking action in the middle troposphere and its effect upon regional climate. II. The climatology of blocking action. *Tellus 2*, 275–301.

Saltzman, B. 1970. Large-scale atmospheric energetics in the wave number domain. *Rev. Geophys. Space. Phys. 8*, 289–302.

Schubert, S. D. 1986. The structure, energetics and evolution of the dominant frequency-dependent three dimensional atmospheric modes. *J. Atmos. Sci. 43*, 1210–1237.

Sheng, J. 1986. On the energetics of low frequency motions. Ph. D. dissertation. Department of Meteorology, Florida State University, Tallahassee, Florida. 186 pp.

Sheng, J. and Hayashi, Y. 1990a. Estimation of atmospheric energetics in the frequency domain during the FGGE year. *J. Atmos. Sci. 47*, 1255–1268.

Sheng, J. and Hayashi, Y. 1990b. Observed and simulated energy cycles in the frequency domain. *J. Atmos. Sci. 47*, 1243–1254.

Shutts, G. J. 1983. The propagation of eddies in diffluent jetstreams: eddy vorticity forcing of "blocking" flow fields. *Quart. J. R. Met. Soc. 109*, 737–761.

Simmons, A. J. and Hoskins, B. J. 1978. The life cycles of some nonlinear baroclinic waves. *J. Atmos. Sci. 35*, 414–432.

Simmons, A. J., Wallace, J. M. and Branstator, G. W. 1983. Barotropic wave propagation and instability, and atmospheric teleconnection patterns. *J. Atmos. Sci. 40*, 1363–1392.

Trenberth, K. E. and Olson, J. G. 1988. An evaluation and intercomparison of global analyses from the National Meteorological Center and the European Centre for Medium Range Weather Forecasts. *Bull. Amer. Meteor. Soc. 69*, 1047–1057.

Wallace, J. M. and Lau, N.-C. 1985. On the role of barotropic energy conversion in the general circulation. *Adv. Geophys. 28A*, 33–74.